







RESEARCH ARTICLE | SEPTEMBER 11 2023

## Linear magnetoelectric coupling and type-II multiferroic order in $\text{NiMn}_2\text{O}_4$

A. Chatterjee ; A. Kumar ; P. K. Manna; S. Bedanta ; A. Sarma ; S. Majumdar; S. M. Yusuf ; S. Giri  



*J. Appl. Phys.* 134, 104103 (2023)

<https://doi.org/10.1063/5.0149744>

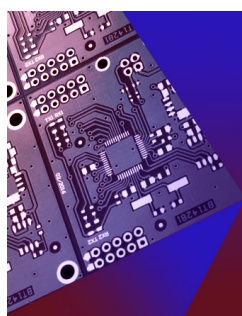


View  
Online



Export  
Citation

CrossMark



### APL Electronic Devices

CALL FOR APPLICANTS

## Seeking Editor-in-Chief



AIP  
Publishing

# Linear magnetoelectric coupling and type-II multiferroic order in $\text{NiMn}_2\text{O}_4$

Cite as: J. Appl. Phys. **134**, 104103 (2023); doi: [10.1063/5.0149744](https://doi.org/10.1063/5.0149744)

Submitted: 2 June 2023 · Accepted: 7 August 2023 ·

Published Online: 11 September 2023



A. Chatterjee,<sup>1</sup> A. Kumar,<sup>2</sup> P. K. Manna,<sup>3,a)</sup> S. Bedanta,<sup>3</sup> A. Sarma,<sup>4</sup> S. Majumdar,<sup>1</sup> S. M. Yusuf,<sup>2</sup> and S. Giri<sup>1,b)</sup>

## AFFILIATIONS

<sup>1</sup>School of Physical Sciences, Indian Association for the Cultivation of Science, Jadavpur, Kolkata 700032, India

<sup>2</sup>Solid State Physics Division, Bhabha Atomic Research Centre, Mumbai 400085, India and Homi Bhabha National Institute, Anushaktinagar, Mumbai 400094, India

<sup>3</sup>Laboratory for Nanomagnetism and Magnetic Materials (LNMM), School of Physical Sciences, National Institute of Science Education and Research (NISER), An OCC of Homi Bhabha National Institute (HBNI), Jatni, 752050 Odisha, India

<sup>4</sup>Deutsches Elektronen-Synchrotron DESY, Notkestr. 85, 22603 Hamburg, Germany

<sup>a)</sup>**Present address:** TERI-Deakin Nanobiotechnology Centre, TERI Gram, The Energy and Resources Institute (TERI), Gual Pahari, Gurgaon Faridabad Road, Gurgaon, Haryana 122 001, India

<sup>b)</sup>**Author to whom correspondence should be addressed:** [sspsg2@iacs.res.in](mailto:sspsg2@iacs.res.in)

## ABSTRACT

We report an unexplored type-II multiferroic order in  $\text{NiMn}_2\text{O}_4$ , exhibiting strong linear magnetoelectric coupling above liquid-nitrogen (LN) temperature. The compound becomes ferroelectric at  $\sim 100$  K, coinciding with ferrimagnetic ordering, with a polarization value of  $\sim 535 \mu\text{C}/\text{m}^2$  for a poling field of  $5 \text{ kV}/\text{cm}$ . At LN temperature, the polarization value increases linearly ( $\sim 21\%$ ) with a magnetic field up to  $30 \text{ kOe}$ . Rietveld refinement of neutron diffraction patterns reveals a ferrimagnetic model with antiparallel moments at tetrahedral and octahedral sites, as well as a canting of octahedral moment persisting up to  $\sim 100$  K. Low-temperature synchrotron diffraction confirms a step-like oxygen displacement during multiferroic ordering, suggesting that the Dzyaloshinskii-Moriya interaction polarizes the intervening oxygen atoms through magnetostriction, providing a microscopic mechanism for spontaneous electric polarization in this linear magnetoelectric multiferroic compound.

Published under an exclusive license by AIP Publishing. <https://doi.org/10.1063/5.0149744>

## I. INTRODUCTION

Current research in magnetoelectric (ME) multiferroics focuses on identifying promising candidates that exhibit strong ME coupling at higher temperatures.<sup>1,2</sup> While there is growing interest in investigating chemically single-phase compounds that exhibit coexistence of mutually exclusive order parameters in multiferroics,<sup>3,4</sup> achieving a strong ME coupling close to room temperature is considered promising for technological applications.<sup>5–8</sup> The linear ME effect, which involves multiferroicity, offers additional degrees of freedom and is beneficial for applications in various sectors such as spintronics, nonvolatile memories, and magnetic field sensors.<sup>9–11</sup>

The spinel compound  $\text{NiMn}_2\text{O}_4$  (NMO) has garnered significant attention for its potential applications, including photocatalytic activity in NMO films,<sup>12</sup> high-performance supercapacitors,<sup>13</sup>

gas sensors,<sup>14</sup> and thermistors.<sup>15</sup> The influence of the antisite disorder has been reported for NMO, where an inversion parameter ( $\bar{\nu}$ ) was defined in  $(\text{Ni}_{1-\bar{\nu}}^{2+}\text{Mn}_{\bar{\nu}}^{2+})[\text{Ni}_{\bar{\nu}}^{2+}\text{Mn}_{2(1-\bar{\nu})}^{3+}\text{Mn}_{\bar{\nu}}^{4+}]\text{O}_4$ .<sup>16</sup> The ions in the first and third brackets occupy tetrahedral and octahedral sites, respectively. Microwave irradiation was found to have a more pronounced effect on tuning the  $\bar{\nu}$  parameter compared to annealing conditions.<sup>17</sup> The tuning of magnetic ordering temperatures through  $\bar{\nu}$  has been reported within a certain range of  $\sim 100$ – $145$  K for  $\text{NiMn}_2\text{O}_4$ .<sup>18–23</sup> The antisite disorder has been further confirmed from the neutron diffraction studies.<sup>24–27</sup> A modified magnetic ground state was proposed for the epitaxial  $\text{NiMn}_2\text{O}_4$  film,<sup>28</sup> unlike the bulk counterpart.

In this article, we present unexplored emergence of spontaneous ferroelectric (FE) polarization below the established ferrimagnetic

17 January 2024 10:17:12

order ( $T_C$ ), suggesting NMO as a type-II multiferroic order.<sup>1,29</sup> The saturation value of the FE polarization ( $P_S$ ) is found to be  $\sim 535 \mu\text{C}/\text{m}^2$  in the as-synthesized air annealed sample, with a poling field of  $5 \text{ kV}/\text{cm}$ . Intriguingly, this value is reduced to  $\sim 182 \mu\text{C}/\text{m}^2$  upon  $\text{O}_2$  annealing. Rietveld refinements of the neutron diffraction patterns propose a canted magnetic structure with a ferrimagnetic model describing antiparallel ordering of moments at the tetrahedral  $[8a \ (1/8, 1/8, 1/8)]$  and the octahedral  $[16d \ (1/2, 1/2, 1/2)]$  sites in the crystal structure for the air annealed sample. It is worth noting that the canted magnetic moment persists at the octahedral site up to  $T_C$  around  $100 \text{ K}$ . The Dzyaloshinskii-Moriya (DM) interaction-induced canted spin configuration, occurring below  $T_C$ , breaks the space inversion symmetry and leads to the observed ferroelectric order in NMO.

## II. EXPERIMENTAL DETAILS

Polycrystalline  $\text{NiMn}_2\text{O}_4$  was prepared using the solid state reaction method.<sup>18</sup>  $\text{NiO}$  and  $\text{Mn}_2\text{O}_3$  were taken in appropriate ratio, thoroughly mixed, and then heated at  $1000^\circ\text{C}$  for  $24 \text{ h}$  in air to obtain the air annealed sample. A portion of this air annealed sample further heated at  $1000^\circ\text{C}$  for  $24 \text{ h}$  in oxygen atmosphere.

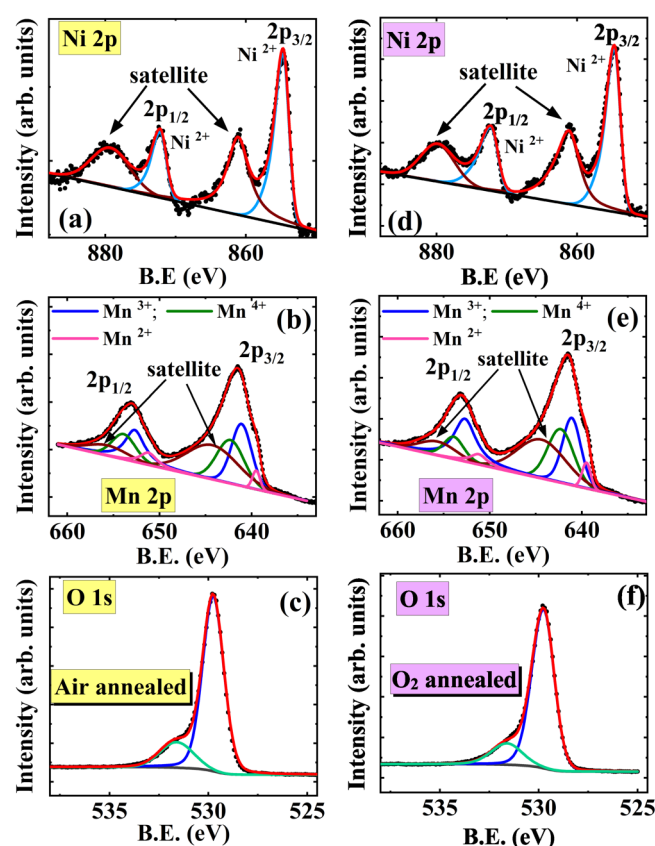


FIG. 1. XPS spectra of (a) Ni, (b) Mn, and (c) O for air annealed and (d) Ni, (e) Mn, and (f) O for  $\text{O}_2$  annealed sample.

Single-phase chemical composition was confirmed by the x-ray diffraction studies at room temperature recorded using a PANalytical x-ray diffractometer (Model: X'Pert PRO) using  $\text{Cu K}\alpha$  radiation. Synchrotron diffraction studies were conducted at P21.1 beamline of PETRA III, Hamburg, Germany, where a two-dimensional (2D) Perkin Elmer detector was used and the wavelength employed was  $0.1221 \text{ \AA}$ . X-ray photoemission spectroscopy (XPS) is recorded with a spectrometer of Omicron Nanotechnology. dc magnetization was measured using a commercial vibrating sample magnetometer of Quantum Design (MPMS, evercool), and pyroelectric current was recorded in a home-built probe attached to a PPMS-II of Quantum Design. Temperature-dependent neutron diffraction experiments were carried at powder diffractometer  $-1$  ( $1.094 \text{ \AA}$ ), Dhruva reactor, Bhabha Atomic Research Centre (BARC), Mumbai, India. All diffraction patterns were analyzed by the Rietveld refinement.<sup>30</sup>

## III. EXPERIMENTAL RESULTS AND DISCUSSIONS

The XPS spectra of the air annealed and  $\text{O}_2$  annealed samples are shown in Figs. 1(a–c) and 1(d–f), respectively. The deconvoluted components of  $2p_{3/2}$ ,  $2p_{1/2}$ , and satellite peaks for Ni are shown in Figs. 1(a) and 1(d) for the air and  $\text{O}_2$  annealed samples, respectively. The deconvoluted peaks of Mn consisting of  $\text{Mn}^{2+}$ , major  $\text{Mn}^{3+}$ , and  $\text{Mn}^{4+}$  components are also depicted in Figs. 1(b) and 1(e) for the air and  $\text{O}_2$  annealed samples, respectively. The spectra for O are depicted in Figs. 1(c) and 1(f) for the air and  $\text{O}_2$  annealed samples, respectively. The ratios between anions and cations, as obtained from the total area of atoms, remain nearly unchanged. However, the ratio between  $\text{Mn}^{2+} : \text{Mn}^{3+}$  increases slightly from  $1 : 5.2$  to  $1 : 5.4$ , respectively, for the air and  $\text{O}_2$  annealed samples. The results indicate that oxygen annealing influences the ratio between the Mn ions.

Thermal variations of dc magnetization recorded at  $50 \text{ Oe}$  after cooling in zero-field cooled (ZFC) and field-cooled (FC) conditions are depicted in Figs. 2(a) and 2(b) for the air and  $\text{O}_2$  annealed samples, respectively. These figures illustrate a sharp rise in magnetization ( $M$ ) at the ferrimagnetic ordering temperatures around  $\sim 100$  and  $\sim 102.5 \text{ K}$  for the air and  $\text{O}_2$  annealed NMO, respectively. The  $dM_{\text{ZFC}}/dT$  plots with respect to temperature ( $T$ ) are also shown in Figs. 2(a) and 2(b) for the air and  $\text{O}_2$  annealed samples, respectively, which further confirms the values of  $T_C$  at the sharp minima of the plots. The determined values of  $T_C$  are close to the low end of the reported  $T_C$  range of approximately  $100\text{--}145 \text{ K}$ , which has been correlated with different ratios between the  $\text{Ni}^{2+}$ ,  $\text{Mn}^{2+}$ ,  $\text{Mn}^{3+}$ , and  $\text{Mn}^{4+}$  content.<sup>18–23</sup> In accordance with the previous reports, a shoulder ( $T_M$ ) is observed in ZFC magnetization below  $T_C$ . The thermal variations of the ac susceptibility measurements for both the samples also exhibit a shoulder, which corresponds to the shoulder observed in dc magnetization. However, no significant shift of  $T_M$  is observed at different frequencies. These results suggest the possibility of domain dynamics associated with the emergence of the shoulder. The origin of this phenomenon requires further clarification through microscopic experimental tools.

We recorded the pyroelectric current ( $I_p$ ) for different poling temperatures ( $T_{\text{pole}}$ ) with the  $\pm 5 \text{ kV}/\text{cm}$  poling field ( $E$ ) and

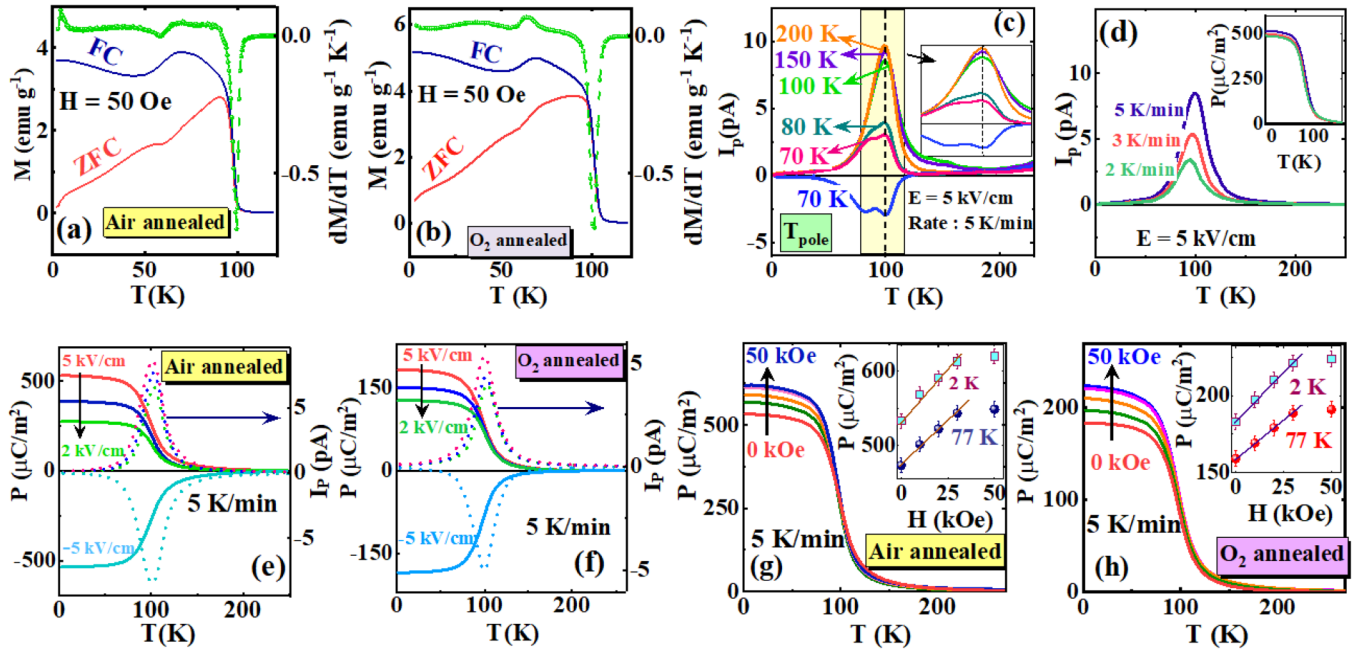


**FIG. 2.** Thermal variations of FC-ZFC magnetization (left axis) and  $dM/dT$  (right axis) for air (a) and  $O_2$ , (b) annealed NMO, (c)  $I_p$  for different poling temperatures ( $T_{pole}$ ), as shown in the figure, (d)  $I_p$  for different sweeping rates,  $P$  and  $I_p$  for different  $E$  for (e) air and (f)  $O_2$  annealed NMO,  $P$  for different  $H$  for (g) air and (h)  $O_2$  annealed NMO. The inset of (c) magnifies the highlighted region, where the broken straight line indicates FE ordering temperature ( $T_{FE}$ ). The inset of (d) depicts thermal variation of  $P$  for different thermal sweeping rates. Variation of  $P$  with  $H$  at selective temperatures in the insets of (g) air and (h)  $O_2$  annealed NMO, where straight lines guide linearity of the plots.

thermal sweeping rate of 5 K/min for the air annealed NMO. In this setup, the sample is always cooled from the selected  $T_{pole}$  down to 2 K and  $I_p$  is recorded during the warming mode without any electric field. The results of  $I_p(T)$  for different  $T_{pole}$  are presented in Fig. 2(c) for a heating rate of 5 K/min. Different  $T_{pole}$  values are chosen as representatives of poling temperatures below, above, and close to approximately 100 K, where a peak is observed in  $I_p(T)$ . In all cases, the peak is consistently observed near  $T_C$ , as indicated by the broken straight line in the inset of Fig. 2(c). When  $T_{pole}$  is selected below  $T_C$ , an additional peak emerges close to  $T_{pole}$ , resulting in a double peak in  $I_p(T)$ . The peak observed at  $T_{pole}$  represents an extrinsic component. On the other hand, when  $T_{pole}$  is chosen above  $T_C$ , a shoulder is observed in  $I_p(T)$  around 150 K, in addition to the intrinsic peak at  $T_C$  for  $T_{pole} = 150$  K. The high- $T$  shoulder disappears, when  $T_{pole}$  is chosen much above  $T_C$  such as 200 K. These results suggest that additional peaks at high and low temperatures are attributed to extrinsic thermally stimulated depolarization currents (TSDCs).<sup>31–34</sup> Thus, the clear signature of a peak observed close to  $T_C$  around 100 K confirms the genuine occurrence of the polar order at  $T_{FE}$ . The  $I_p(T)$  curve for  $T_{pole} = 70$  K and  $-5$  kV/cm is also displayed in the figure, where the reversing of  $I_p(T)$  due to change in sign of the poling electric field demonstrates the FE order. For the calculation of  $P(T)$ , the  $I_p(T)$  recorded for  $T_{pole} = 200$  K is utilized. The  $I_p(T)$  recorded at different heating rates is shown in Fig. 2(d). Integrating  $I_p(T)$  over time yields  $P(T)$ ,

which nearly reproduces the same  $P(T)$  curve, as depicted in the inset of the figure. These results indicate that the trapped charges do not contribute to  $I_p(T)$ . The  $P(T)$  curves recorded for different poling fields from 2 to 5 kV/cm are illustrated in Figs. 2(e) and 2(f) for the air-annealed and  $O_2$ -annealed NMO, respectively. In case of air-annealed NMO, the saturated value of  $P$  is  $535 \mu\text{C}/\text{m}^2$  for  $E = 5$  kV/cm, which is significantly larger compared to the values reported for promising type-II multiferroics.<sup>29,36–38</sup> However, the value of  $P$  reduces remarkably to  $182 \mu\text{C}/\text{m}^2$  after  $O_2$  annealing.

The  $P(T)$  values are recorded for different  $H$  for both the samples, as depicted in Figs. 2(g) and 2(h). The  $P(T)$  increases significantly upon application of  $H$  below  $T_{FE}$ . The variations of  $P$  with  $H$  for selective temperatures at 2 and 77 K are shown in the corresponding insets. In both cases, the  $P$  increases almost linearly with  $H$ , as indicated by the straight lines until approximately 30 kOe, beyond which it saturates up to  $H \approx 50$  kOe. The change of  $P$  indicates the presence of linear ME coupling, which is considerable, reaching approximately  $\sim 17\%$  and  $\sim 21\%$  for the air-annealed and  $O_2$ -annealed NMO, respectively, at the liquid-nitrogen temperature with  $H = 30$  kOe. The linear ME is promising and has been observed in few systems such as  $\text{Sm}_2\text{BaCuO}_5$ <sup>39,40</sup> and  $\text{Fe}_3\text{Mo}_3\text{O}_8$ .<sup>41</sup> It is noteworthy that the ME coupling remains significant in the current observation at liquid-nitrogen temperature for a magnetic field, which can be achieved using an electromagnet.

The synchrotron diffraction patterns were recorded in the range of 15–200 K and Rietveld refinements were performed for all temperatures. The refinement of the diffraction pattern at 300 K is illustrated in Fig. 2(a) using space group  $Fd\bar{3}m$ ,  $Z = 8$ .<sup>21,24–27</sup> An example of the refinement below  $T_C$  or  $T_{FE}$  at 18 K is shown in Fig. 3(b). The reliability parameters are as follows:  $R_w$  (%)  $\approx 4.85$ ,  $R_{exp}$  (%)  $\approx 1.15$ , and  $\sigma \approx 3.04$  for the refinement at 300 K and  $R_w$  (%)  $\approx 4.15$ ,  $R_{exp}$  (%)  $\approx 1.17$ , and  $\sigma \approx 2.4$  for the refinement at 18 K. Throughout the recorded temperature range, the diffraction data are satisfactorily refined using  $Fd\bar{3}m$  space group, consistent with the findings of previous report.<sup>21</sup> Integrated intensity of a (220) peak, shown in Fig. 3(c) as a function temperature, exhibits anomalies near  $T_{FE}$  or  $T_C$  and  $T_M$ , indicating magnetoelastic coupling. In the  $Fd\bar{3}m$  structure, the positions of Ni and Mn are fixed, while the positions of oxygen atoms vary with temperature. The variation of oxygen position as a function of temperature is shown in Fig. 3(d), revealing anomalies at  $T_{FE}$  and near  $T_M$ . Consistent with these results, the lattice constant ( $a$ ) decreases with temperature, displaying anomalies at  $T_{FE}$  and near  $T_M$ , as depicted in Fig. 3(e).

To conclude, the neutron diffraction studies were conducted on the air-annealed compound in the temperature range of 5–300 K. Rietveld refinements of the neutron diffraction patterns are depicted at 300 and 5 K in Figs. 4(a) and 4(b), respectively. The refinement of the 300 K reveals a cation distribution for  $NiMn_2O_4$  as  $(Mn_{0.92}Ni_{0.08})^{Tetra}[Mn_{0.54}Ni_{0.46}]_2^{Octa}O_4$ , indicating a significant anti-site disorder. The terms “Tetra” and “Octa” in the superscript of the formula represent the tetrahedral and octahedral sites, respectively. The neutron diffraction patterns recorded below  $\sim 100$  K show enhanced intensities of the fundamental (nuclear) Bragg peaks without appearance of any additional peaks. This suggests a ferrimagnetic model with antiparallel ordering of the

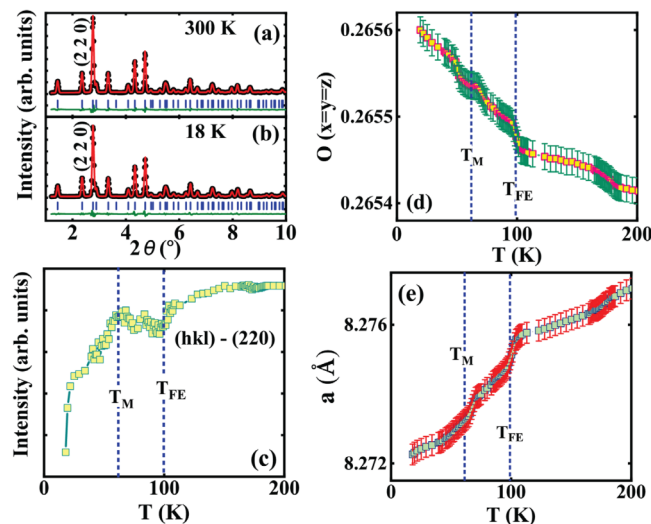


**FIG. 3.** Rietveld refinement of diffraction patterns at (a) 300 K and (b) 18 K for the air annealed sample. Thermal variations of (c) integrated intensity of the (220) peak, (d) oxygen displacement, (e) lattice constant ( $a$ ).

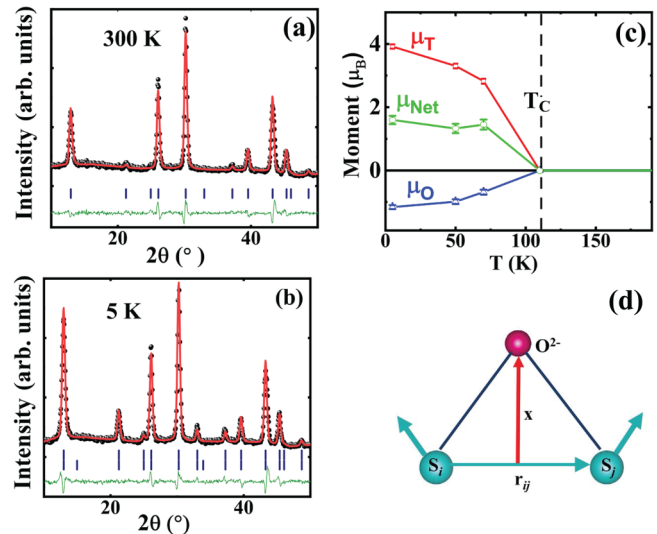


**FIG. 4.** Rietveld refinement of the neutron diffraction patterns at (a) 300 K and (b) 5 K. (c)  $T$  variations of the moment at the tetrahedral ( $\mu_T$ ), octahedral ( $\mu_O$ ) sites, and net moment ( $\mu_{Net}$ ). (d) Possible direction of  $O^{2-}$  ion along  $x$  driven by DM interaction between  $i$ th ( $S_i$ ) and  $j$ th ( $S_j$ ) spins according to DM model.

moments at the tetrahedral [8a (1/8, 1/8, 1/8)] and the octahedral [16d (1/2, 1/2, 1/2)] sites, aligned along the crystallographic axes. The variations of octahedral ( $\mu_T$ ), tetrahedral ( $\mu_O$ ), and net ( $\mu_{Net}$ ) magnetic moments with  $T$  are depicted in Fig. 4(c), displaying behavior typical of a ferrimagnetic system. The moment at the octahedral site is considerably smaller than the expected spin only value corresponding to Mn and Ni cations residing at the octahedral site, as determined from the Rietveld refinements. This indicates a canting of the octahedral site moments. Our neutron diffraction results provide further evidence of the canted magnetic structure of  $NiMn_2O_4$ , persisting up to  $T_C$  at 100 K, which correlates with the occurrence of ferroelectric order. The  $O_2$  annealing of the sample reduces the  $Mn^{2+} : Mn^{3+}$  ratio and promotes less spin canting at the octahedral site, resulting in a decrease in polarization. The derived octahedral site moment in our neutron diffraction study only corresponds to the ordered (longitudinal) component of the B-site moment. The spatial ordering of the transverse component of the B-site moment would manifest as the (200) Bragg reflection, which is completely absent in the neutron diffraction patterns. These results indicate that the transverse component of the octahedral site moment is not ordered. The possible canting of the tetrahedral moments can be inferred from the cation distribution of NMO from the Rietveld refinements. It is noteworthy that the calculated moment value is close to the observed moment of  $\sim 3.9 \mu_B$  at 5 K, suggesting the almost absence of spin canting at the tetrahedral site.

The Dzyaloshinskii–Moriya (DM) interaction induces spin canting of the octahedral moments at the onset of  $T_C$ . In case of FE polarization driven by the DM interaction, the spin-current model suggests the possibility of polarization.<sup>42</sup> According to this

17 January 2024 10:17:12



model, the DM interaction can induce ferroelectric polarization of the electronic orbitals without involving lattice distortion. However, low temperature synchrotron diffraction studies reveal an isostructural lattice distortion at the onset of the FE order, indicating that the spin-current model may not be applicable in the current context. Another interpretation involves the inverse DM interaction, which provides a microscopic mechanism for the strong coupling between ferroelectricity and magnetism. In this interpretation, the DM interaction can polarize an oxygen (ligand) atom through magnetostriction, resulting in electric polarization.<sup>43</sup> The antisymmetric DM interaction is described as  $D_{ij} \cdot S_i \times S_j$ , where  $D_{ij} = x \times r_{ij}$  is the Dzyaloshinskii vector and  $x$  is perpendicular to  $r_{ij}$ , as described in Fig. 4(d). In this context, the stronger DM interaction pushes oxygen atoms along the  $x$  direction. As depicted in 3(d), a nearly step-like oxygen displacement supports the interpretation based on the inverse DM interaction. This observed phenomenon is analogous to what has been proposed in different systems,<sup>36,44</sup> including other spinel oxides such as  $\text{CoCr}_2\text{O}_4$ <sup>45</sup> and  $\text{MnCr}_2\text{O}_4$ .<sup>46</sup>

#### IV. CONCLUSION

Our studies in  $\text{NiMn}_2\text{O}_4$  reveal an unexplored multiferroic order at the ferrimagnetic ordering temperature. Significant magnetoelectric coupling of 17%–21% is observed at liquid nitrogen temperature, when applying a magnetic field of 30 kOe, which can be achieved using an electromagnet. Synchrotron diffraction measurements confirm a step-like isostructural transition with a corresponding step-like displacement of oxygen atoms at  $T_{FE}$ . Neutron diffraction studies demonstrate the persistence of spin canting at the octahedral sites up to  $T_C$ . The occurrence of spin canting, attributed to the Dzyaloshinskii–Moriya interaction, is proposed to polarize the oxygen atoms through magnetostriction, resulting in spontaneous electric polarization at  $T_C$ .<sup>47,48</sup>

#### ACKNOWLEDGMENTS

S.G. acknowledges SERB (Project No.: CRG/2022/000718) for the financial support and DST, India for the financial support to perform experiment at PETRA III, DESY, Germany for synchrotron diffraction studies (Proposal No.: I20200322). S.B. acknowledges the financial support from Department of Atomic Energy (DAE) of Government of India.

#### AUTHOR DECLARATIONS

##### Conflict of Interest

The authors have no conflicts to disclose.

##### Author Contributions

**A. Chatterjee:** Formal analysis (lead); Investigation (lead). **A. Kumar:** Conceptualization (equal); Formal analysis (lead); Supervision (equal); Writing – original draft (equal). **P. K. Manna:** Investigation (equal). **S. Bedanta:** Supervision (equal). **A. Sarma:** Investigation (equal). **S. Majumdar:** Conceptualization (equal); Supervision (equal). **S. M. Yusuf:** Conceptualization (equal); Supervision (equal). **S. Giri:** Conceptualization (lead); Supervision

(lead); Writing – original draft (lead); Writing – review & editing (lead).

#### DATA AVAILABILITY

The data that support the findings of this study are available from the corresponding author upon reasonable request.

#### REFERENCES

- <sup>1</sup>M. Fiebig, T. Lottermoser, D. Meier, and M. Trassin, *Nat. Rev. Mater.* **1**, 16046 (2016).
- <sup>2</sup>N. A. Spaldin and R. Ramesh, *Nat. Mater.* **18**, 203 (2019).
- <sup>3</sup>M. Giraldo, Q. N. Meier, A. Bortis, D. Nowak, N. A. Spaldin, M. Fiebig, M. C. Weber, and T. Lottermoser, *Nat. Commun.* **12**, 3093 (2021).
- <sup>4</sup>Y. Geng, H. Das, A. L. Wysocki, X. Wang, S.-W. Cheong, M. Mostovoy, C. J. Fennie, and W. Wu, *Nat. Mater.* **13**, 163 (2014).
- <sup>5</sup>X. Zhao, D. Wang, H. Zhang, L. Liu, H. Lin, Z. Wang, X. Zhang, C. Xie, W. Lin, N. Gao, C. Pan, and G. Xing, *J. Appl. Phys.* **132**, 084902 (2022).
- <sup>6</sup>X. Liang, H. Chen, and N. X. Sun, *APL Mater.* **9**, 041114 (2021).
- <sup>7</sup>S. Kopyl, R. Surmenev, M. Surmeneva, Y. Fetisov, and A. Kholkin, *Mater. Today Bio.* **12**, 100149 (2021).
- <sup>8</sup>L. Lin, Y. S. Tang, L. Huang, W. J. Zhai, G. Z. Zhou, J. H. Zhang, M. F. Liu, G. Y. Li, X. Y. Li, Z. B. Yan, and J.-M. Liu, *Appl. Phys. Lett.* **120**, 052901 (2022).
- <sup>9</sup>S. Fusil, V. Garcia, A. Barthélémy, and M. Bibes, *Annu. Rev. Mater. Res.* **44**, 91 (2014).
- <sup>10</sup>N. Ortega, A. Kumar, J. F. Scott, and R. S. Katiyar, *J. Phys.: Condens. Matter* **27**, 504002 (2015).
- <sup>11</sup>A. K. Singh, S. D. Kaushik, B. Kumar, P. K. Mishra, A. Venimadhav, V. Siruguri, and S. Patnaik, *Appl. Phys. Lett.* **92**, 132910 (2008).
- <sup>12</sup>T. Larbi, K. Doll, and M. Amlouk, *Spectrochim. Acta A Mol. Biomol. Spectrosc.* **216**, 117 (2019).
- <sup>13</sup>H. Nan, W. Ma, Z. Gu, B. Geng, and X. Zhang, *RSC Adv.* **5**, 24607 (2015).
- <sup>14</sup>Y. Guan, C. Yin, X. Cheng, X. Liang, Q. Diao, H. Zhang, and G. Lu, *Sens. Actuators B Chem.* **193**, 501 (2014).
- <sup>15</sup>M. Parlak, T. Hashemi, M. J. Hogan, and A. W. Brinkman, *Thin Solid Films* **345**, 307 (1999).
- <sup>16</sup>V. A. M. Brabers, F. M. Van Setten, and P. S. A. Knapen, *J. Solid State Chem.* **49**, 93 (1983).
- <sup>17</sup>H. Goto, J. Fukushima, and H. Takizawa, *Materials* **9**, 169 (2016).
- <sup>18</sup>P. N. Lisboa-Filho, M. Bahout, P. Barahona, C. Moure, and O. Peña, *J. Phys. Chem. Solids* **66**, 1206 (2005).
- <sup>19</sup>A. Díez, R. Schmidt, A. E. Sagua, M. A. Frechero, E. Matesanz, C. Leon, and E. Morán, *J. Eur. Ceram. Soc.* **30**, 2617 (2010).
- <sup>20</sup>M. Tadic, S. M. Savic, Z. Jaglicic, K. Vojislavljivic, A. Radojkovic, S. Prsic, and D. Nikolic, *J. Alloys Compd.* **588**, 465 (2014).
- <sup>21</sup>S. Asbrink, A. Waśkowska, M. Drozd, and E. Talik, *J. Phys. Chem. Solids* **58**, 725 (1997).
- <sup>22</sup>A. J. Freitas Cabral, C. M. R. Remédios, X. Gratens, and V. A. Chitta, *J. Magn. Mater.* **469**, 108 (2019).
- <sup>23</sup>A. J. Freitas Cabral, J. D. Peña, B. R. Salles, H. S. Amorim, C. M. R. Remédios, and M. A. Novak, *J. Magn. Mater.* **538**, 168291 (2021).
- <sup>24</sup>P. B. Boucher, R. Buhl, and E. M. Perrin, *Acta Cryst. B* **25**, 2326 (1969).
- <sup>25</sup>J. L. Baudour, R. Buhl, and M. Perrin, *J. Phys. Chem. Solids* **31**, 363 (1970).
- <sup>26</sup>J. L. Baudour, F. Bouree, M. A. Fremy, R. Legros, A. Rousset, and B. Gillot, *Phys. B* **180 & 181**, 97 (1992).
- <sup>27</sup>A. Sagua, G. M. Lescano, J. A. Alonso, R. Martínez-Coronado, M. T. Fernández-Díaz, and E. Morán, *Mater. Res. Bull.* **47**, 1335 (2012).
- <sup>28</sup>B. B. Nelson-Cheeseman, R. V. Chopdekar, J. M. Iwata, M. F. Toney, E. Arenholz, and Y. Suzuki, *Phys. Rev. B* **82**, 144419 (2010).
- <sup>29</sup>D. Khomskii, *Physics* **2**, 20 (2009).
- <sup>30</sup>H. M. Rietveld, *J. Appl. Crystallogr.* **2**, 65 (1969).
- <sup>31</sup>T. N. M. Ngo, U. Adem, and T. T. M. Palstra, *Appl. Phys. Lett.* **106**, 152904 (2015).

- <sup>32</sup>N. Terada, Y. S. Glazkova, and A. A. Belik, *Phys. Rev. B* **93**, 155127 (2016).
- <sup>33</sup>R. Chen and Y. Kirsh, *Analysis of Thermally Stimulated Process* (Pergamon, New York, 1981).
- <sup>34</sup>W. Liu and C. A. Randall, *J. Am. Ceram. Soc.* **91**, 3245 (2008).
- <sup>35</sup>K. Dey, A. Karmakar, A. Indra, S. Majumdar, U. Rütt, O. Gutowski, M. V. Zimmermann, and S. Giri, *Phys. Rev. B* **92**, 024401 (2015).
- <sup>36</sup>J. K. Dey, A. Chatterjee, S. Majumdar, A.-C. Dippel, O. Gutowski, M. V. Zimmermann, and S. Giri, *Phys. B* **99**, 144412 (2019).
- <sup>37</sup>A. Indra, K. Dey, S. Majumdar, I. Sarkar, S. Francoual, R. P. Giri, N. Khan, P. Mandal, and S. Giri, *Phys. Rev. B* **95**, 094402 (2017).
- <sup>38</sup>T. Kimura, Y. Sekio, H. Nakamura, T. Siegrist, and A. P. Ramirez, *Nat. Mater.* **7**, 291 (2008).
- <sup>39</sup>A. Indra, S. Mukherjee, S. Majumdar, O. Gutowski, M. V. Zimmermann, and S. Giri, *Phys. Rev. B* **100**, 014413 (2019).
- <sup>40</sup>P. Yanda, N. V. Ter-Oganessian, and A. Sundaresan, *Phys. Rev. B* **100**, 104417 (2019).
- <sup>41</sup>T. Kurumaji, S. Ishiwata, and Y. Tokura, *Phys. Rev. X* **5**, 031034 (2015).
- <sup>42</sup>H. Katsura, N. Nagaosa, and A. V. Balatsky, *Phys. Rev. Lett.* **95**, 057205 (2005).
- <sup>43</sup>I. A. Sergienko and E. Dagotto, *Phys. Rev. B* **73**, 094434 (2006).
- <sup>44</sup>H. J. Zhao, P. Chen, S. Prosandeev, S. Artyukhin, and L. Bellaiche, *Nat. Mater.* **20**, 341 (2021).
- <sup>45</sup>Y. Yamasaki, S. Miyasaka, Y. Kaneko, J.-P. He, T. Arima, and Y. Tokura, *Phys. Rev. Lett.* **96**, 207204 (2006).
- <sup>46</sup>K. Dey, S. Majumdar, and S. Giri, *Phys. Rev. B* **90**, 184424 (2014).
- <sup>47</sup>M. E. Lines and A. M. Glass, *Principles and Applications of Ferroelectrics and Related Materials* (Clarendon Press, Oxford, 1997).
- <sup>48</sup>K. Dey, A. Karmakar, A. Indra, S. Majumdar, U. Rütt, O. Gutowski, M. V. Zimmermann, and S. Giri, *Phys. Rev. B* **92**, 024401 (2015).